# GALAXY EVOLUTION IN THE POST-MERGER REGIME. IV - THE LONG-TERM EFFECT OF MERGERS ON GALACTIC STELLAR MASS GROWTH AND DISTRIBUTION

Sara L. Ellison $^1$  and Leonardo Ferreira $^{1,2}$ 

Department of Physics & Astronomy, University of Victoria, Finnerty Road, Victoria, BC V8P 1A1, Canada Instituto de Matemática, Estatística e Física, Universidade Federal do Rio Grande, Brazil Version November 27, 2025

### ABSTRACT

Galaxy mergers are known to trigger bursts of central star formation, which should therefore lead to stellar mass growth in their inner regions. However, observational measurements of this 'burst mass fraction' are scant. Here, we assemble a large ( $\sim 14{,}000$ ) sample of post-coalescence galaxies that have recently completed their merger-induced star formation, and compare various measurements of central stellar mass with a matched control sample. Specifically, we quantify (at fixed redshift, star formation rate and total stellar mass) the stellar mass enhancement within a fixed angular aperture  $(\Delta M_{\star,fibre})$  and in the galactic bulge  $(\Delta M_{\star,bulge})$ , finding burst mass fractions of 10-20 %. 61 galaxies in our sample are at  $z \leq 0.05$  and have integral field unit data from the Mapping Galaxies at Apache Point (MaNGA) survey, allowing further kpc-scale assessment of excess stellar mass and radial gradients. Again, we find a  $\sim 15-20$  % excess of stellar mass in the central regions of the post-mergers compared with matched controls. However, contrary to previous works, which have inferred very compact, centralized merger-induced mass growth, we find a 15 % stellar mass excess out to  $\sim 7$  kpc (1.4  $R_e$  for the stellar masses in our sample). Our work represents the first direct measurement of merger-induced stellar mass that is independent of stellar population modelling, or fitting light profiles, demonstrating significant and extended mass build-up in late stage post-mergers.

### 1. INTRODUCTION

Galaxy mergers represent a cornerstone in the contemporary paradigm of hierarchical growth. The coalescence of two galaxies leads to the natural build-up of all of their constituent parts, from the stars and gas, to their dark matter halos and central supermassive black holes. Merger histories can be witnessed in nearby galaxies in the form of extended low surface brightness features (usually the remnants of relatively major mergers) and stellar streams that result from satellite accretion events (e.g. Karademir et al. 2019; Valenzuela & Remus 2024). However, galactic growth happens in tandem via in-situ processes unrelated to galaxy mergers, for example, as gas is transformed into stars through gravitational collapse in the disk and the central supermassive black hole is fed via secular means. A pertinent question is therefore: what fraction of galaxy growth occurs from star formation enhancement as a direct result of a merger versus secular *in-situ* processes?

In the current paper, we focus on the specific topic of stellar mass growth. Several works have attempted to quantify the fraction of ex-situ stellar mass in galaxies, i.e., the fraction of stellar mass that has been accreted through a merger, rather than formed within the current host. Quantifying the ex-situ stellar mass fraction is relatively straightforward in simulations, whereby the origin of particles can be readily tracked (e.g. Rodriguez-Gomez et al. 2016; Boecker et al. 2023; Cannarozzo et al. 2023). Observationally, quantifying the ex-situ mass fraction is more challenging, but several works have attempted the measurement (Boecker et al. 2020; Angeloudi et al. 2024; 2025; Cai et al. 2025). The general

\*E-mail: sarae@uvic.ca

consensus is that whilst *ex-situ* stellar mass is most readily accreted at larger radii, there is considerable spatial variation due to properties such as mass ratio and dynamics (e.g. Rodriguez-Gomez et al. 2016; Karademir et al. 2019; Angeloudi et al. 2025).

Previous works attempting to quantify the contribution of mergers to stellar mass growth have generally focussed on stars that previously existed in a companion galaxy but that have been accreted during coalescence. I.e. mergers are generally considered to be the source of ex-situ mass. However, this assessment overlooks the fact that star formation occurs as a direct result of the galaxy-galaxy interaction. It is very well documented that galaxy-galaxy interactions lead to enhanced levels of star formation, a process that occurs in both the precoalescence (pair) phase (Ellison et al. 2008; Patton et al. 2013; Scott & Kaviraj 2014) as well as in post-mergers (Ellison et al. 2013; Bickley et al. 2022; Vasquez-Bustos et al. 2025). These stars count neither as in-situ (a term which is usually considered to measure secular star formation) nor ex-situ (accreted from an external source) and are truly 'new' stellar mass spawned by the merger. In the work presented here we aim to quantify this 'new' stellar mass, sometimes referred to as the 'burst mass fraction', that results from interaction-induced enhancements in the star formation rate.

In order to measure the amount of mass in new stars created as a result of a merger, we must know both where and when to look. The spatial location of merger-triggered star formation is predicted by simulations to be central (e.g. Cox et al. 2006; Moreno et al. 2015, 2021). Early observations supported this prediction, either through the measurement of blue centres in mergers (e.g. Ellison et al. 2010; Patton et al. 2011; Lambas et

al. 2012) or the measurement of enhanced star formation rates (SFRs) within small apertures (e.g. Barton, Geller & Kenyon 2000; Lambas et al. 2003; Ellison et al. 2013). Integral field unit (IFU) observations have now firmly established the central nature of triggered star formation (Barrera-Ballesteros et al. 2015; Pan et al. 2019; Thorp et al. 2019; Steffen et al. 2021; Thorp, Ellison & Galicia 2024), informing us that a measurement of newly built stellar mass should be focussed on the inner few kpc.

The question of 'when' to assess the build-up of stellar mass is potentially more tricky. Triggered star formation is known to begin well before coalescence, as demonstrated both in simulations (e.g. Perez et al. 2006; Cox et al. 2008; Torrey et al. 2012; Patton et al. 2020) and the presence of enhanced SFRs in the pair phase in observations (Nikolic, Cullen & Alexander 2004; Ellison et al. 2008; Barton et al. 2010; Patton et al. 2013). However, this is just the start of the process and any measurement of stellar mass build-up in the pair phase will not capture the full extent of the growth. Indeed, observationally, SFRs seem to peak in the post-merger regime (Ellison et al. 2013; Bickley et al. 2022), but how long does this enhancement persist after coalescence? Knowing the answer to this question is critical, so that we can measure the central stellar mass excess once the epoch of triggered star formation is completed and a full accounting of new mass production can be made.

Previously, our only guidance for the timescale over which star formation rates remained enhanced came from simulations, which predicted that SFRs returned to normal  $\sim 0.5$  – 1 Gyr after coalescence (Hani et al. 2020; Schechter et al. 2025). However, recently we have obtained a direct observational measurement of the evolution of SFR enhancement as a function of time. Thanks to machine vision informed predictions of time postmerger  $(T_{PM})$ , Ferreira et al. (2025a) have found that SFRs peak around the time of coalescence, but decline to 'normal' values after  $\sim 1$  Gyr, in good agreement with simulations (e.g. Schechter et al. 2025). In order to quantify the mass of new stars formed as a result of mergers we are thus informed to look in the centres of postmerger galaxies that have coalesced around 1 Gyr ago, since these will have recently completed their mergerinduced star formation.

Having established where and when we should measure the burst mass fraction, the final challenge is to identify a sample in which the measurement can be made. As mentioned above, recent advances with machine vision techniques are now making it possible to predict the time before/after coalescence from galaxy morphologies alone (Koppula et al. 2021; Pearson et al. 2024, 2025; Ferreira et al. 2025a,b). Specifically, in the work presented here, we will use the  $T_{PM}$  predictions from the MUlti Model Merger Identifier (MUMMI, Ferreira et al. 2024, 2025b, Ellison et al. in prep; Section 2.1) to identify post-mergers that have recently completed their triggered star formation (Section 2.2). Quantification of excess stellar mass is made via a comparison with a control sample matched in  $M_{\star}$  and redshift (Section 2.3). Burst mass fractions are computed within fixed angular apertures (Section 3.1), within the bulge (Section 3.2) and, for those galaxies observed with the MaNGA IFU

survey, within fixed physical radii and annuli (Section 3.3). We discuss our results in the context of previous observational measurements of the burst mass fraction in Section 4.

#### 2. Data

## 2.1. A brief overview of MUMMI

MUMMI combines an ensemble of 10 convolutional neural networks and 10 vision transformers to yield 20 independent votes on the status of a given galaxy image (Ferreira et al. 2024). MUMMI is trained on labelled images of pre-coalescence pairs, post-mergers and isolated (nonmergers) generated from the Illustris TNG100-1 (hereafter, TNG) simulation (Nelson et al. 2019). Step 1 of MUMMI separates non-mergers and mergers (including both pairs and post-mergers), where the user defines the threshold number of votes (out of a maximum of 20) required for a positive merger classification. Step 2 of MUMMI separates pairs from post-mergers. Full details of the construction and training of Steps 1 and 2 of MUMMI can be found in Ferreira et al. (2024). Step 3 of MUMMI is applied only to post-mergers, and places each galaxy into one of four time post-merger  $(T_{PM})$  bins, up to a maximum of 1.76 Gyr beyond coalescence; see Ferreira et al. (2025b) for more details. Taken together, the three stages of MUMMI are therefore able to not only separate non-mergers from pairs and post-mergers, but also assemble the latter category into a time sequence.

It is well documented that observational realism is important for high performance during machine vision tasks (e.g. Bottrell et al. 2019; Wilkinson et al. 2024). The original MUMMI pipeline was trained using mock realism to match the r-band images of the Ultraviolet Nearinfrared Optical North Survey (UNIONS; Gwyn et al. 2025). However, UNIONS r-band imaging is only available northwards of +30 degrees in declination. In order to maximize the footprint to which MUMMI can be applied, it has subsequently been re-trained for application to the Dark Energy Camera Legacy Survey (DECaLS), providing coverage of more southern declinations (Ellison et al. in prep).

The parent catalog for both MUMMI-UNIONS and MUMMI-DECaLS is based on the main galaxy sample of the Sloan Digital Sky Survey Data Release 7 (SDSS DR7, Abazajian et al. 2009), including galaxies in the redshift range 0.01 < z < 0.3. In order to maximize the post-merger sample used in the current work, we combine the two MUMMI post-merger catalogs, from UNIONS and DECaLS, as described in the next sub-section.

## 2.2. Post-merger selection

Following our previous works (Ferreira et al. 2025a; Ellison et al. 2024, 2025) we identify a galaxy as a post-merger if > 10/20 votes from Step 1 of MUMMI are positive. This majority vote fraction approach has been found to be a good trade-off between completeness and purity (Ferreira et al. 2024). We limit our observational sample to those galaxies with log  $(M_{\star}/M_{\odot}) > 10$ , to reflect the sample on which MUMMI was trained. Stellar masses are taken from the SDSS DR7 MPA/JHU catalog, as described in Kauffmann et al.  $(2003)^{1}$ .

 $<sup>^{1}</sup>$  https://home.strw.leidenuniv.nl/ $\sim$ jarle/SDSS/

In the work presented here, our objective is to assess whether there is long term central stellar mass growth as a result of galaxy mergers. We therefore impose two further criteria on the post-merger sample. First, we only use post-mergers in the longest  $T_{PM}$  bin, which corresponds to  $0.96 < T_{PM} < 1.76$  Gyr. The motivation here is to to study galaxies after the merger-induced star formation has been completed. Since Ferreira et al. (2025a) have shown that enhanced SFRs are statistically only found at  $T_{PM} < 0.96$  Gyr, galaxies in the final time bin should be no longer forming excess stars as a result of the merger. Second, we select only post-mergers that are quenched. This second criterion is adopted because we are, once again, interested in measuring the buildup of stellar mass after star formation is complete and there is no further growth. We therefore impose the requirement that the specific SFR (sSFR) be less than log  $sSFR < -11 \text{ yr}^{-1}$ , were SFRs are again taken from the MPA/JHU catalog (Brinchmann et al. 2004). In practice, the longest post-merger time bin is dominated by quenched galaxies (Ellison et al. 2024), such that the majority of galaxies are retained even with the application of this sSFR threshold. As a result of these selection criteria we have a sample of 13,845 quenched post-mergers with log  $(M_{\star}/M_{\odot}) > 10$  and  $0.96 < T_{PM} < 1.76 \text{ Gyr}^2$ , of which approximately two thirds come from DECaLS.

## 2.3. Control matching

In order to identify a matched control sample for the post-mergers, we begin with a pool consisting of all nonmerger galaxies in the UNIONS + DECaLS catalog, defined as having fewer than 3/20 positive votes in Step 1 of MUMMI. For each post-merger we search in turn for every galaxy in the non-merger pool that has the same stellar mass, SFR and redshift within tolerances of 0.05 dex, 0.05 dex and 0.005, respectively. If fewer than five controls are found within these tolerances, we allow them to grow by a further 0.05 dex in both stellar mass and SFR and 0.005 in redshift. The process is repeated a maximum of 5 times, for maximum tolerances in stellar mass, SFR and redshift of 0.25 dex, 0.25 dex and 0.025. In practice, most post-mergers have many tens of matches without any adjustment to the original matching tolerances. Only four post-mergers fail the matching completely and are removed from the sample.

#### 3. RESULTS

We present three complementary experiments to assess whether mergers result in central stellar mass growth.

## 3.1. Enhancements in fibre stellar mass

We begin our assessment of central stellar mass growth by making use of the fibre stellar masses that are provided in the MPA/JHU catalog. The SDSS fibre has a 3 arcsecond diameter, corresponding to an approximate physical size of 1.5 kpc to 5 kpc for the redshift range 0.05 < z < 0.2 over which most of our post-merger sample is located. Despite this variable physical aperture, recall that our control sample is matched in both total stellar mass and redshift. We therefore expect that the

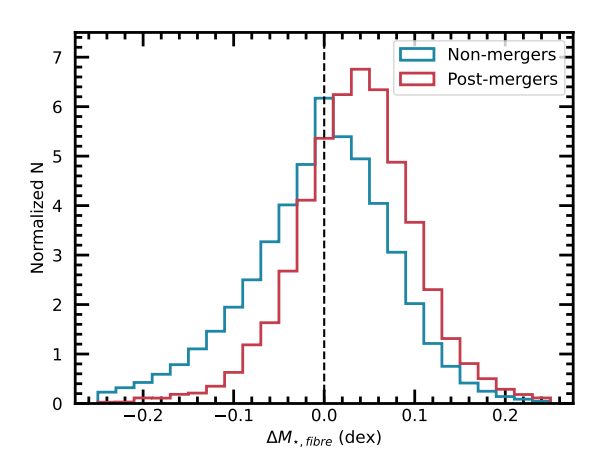


Fig. 1.— Normalized distribution of fibre stellar mass offset  $(\Delta M_{\star,fibre})$  for late-stage (0.96 <  $T_{PM}$  < 1.76 Gyr,) quenched post-mergers (red histogram) and non-mergers (blue). The vertical dashed line is at zero. The median  $\Delta M_{\star,fibre}$  for the post-mergers is 0.04 dex, corresponding to a  $\sim$  10 % enhancement.

control sample for a given post-merger should have aperture coverage of the same physical and relative extent.

We compute a fibre stellar mass 'offset',  $\Delta M_{\star,fibre}$ , as the difference (in log space) between the fibre stellar mass of a given post-merger and the median of its matched controls. As a reference, and to quantify the underlying range in expected  $\Delta M_{\star,fibre}$  in the general galaxy population, it is also possible to compute the fibre mass offset for non-merger galaxies as well. Figure 1 shows the normalized distribution of  $\Delta M_{\star,fibre}$  for the late stage post-mergers (red) and non-mergers (blue). As expected, the non-merger distribution is symmetric and centred around zero. However, for the sample of 13,841 late stage (0.96 <  $T_{PM}$  < 1.76 Gyr) quenched post-mergers, the  $\Delta M_{\star,fibre}$  is skewed towards positive values, with a median of 0.04 dex. Although the magnitude of this median offset is not large (about 10%), the distributions shown in Figure 1 are clearly distinct and the signal of enhanced fibre mass is compelling<sup>3</sup>.

Although the matching in stellar mass and redshift matching takes account of the variable coverage within the fixed 3 arcsecond fibre, Figure 1 nonetheless contains masurements over a range of physical sizes. In order to assess the impact of varying redshift (and hence, varying physical coverage of the fibre), in Figure 2 we plot the median  $\Delta M_{\star,fibre}$  of the post-merger sample in bins of stellar mass and redshift. Figure 2 shows that the enhancement in fibre stellar mass for post-mergers seen in Figure 1 is present across the full stellar mass and redshift range of the sample. However, we note that the enhancement in  $\Delta M_{\star,fibre}$  is slightly smaller (0.03 dex) at stellar masses  $\log (M_{\star}/M_{\odot}) < 11$ . The presence of a fibre mass enhancement even in the highest redshift postmergers in the sample hints that the scale of the stellar mass growth extends to radii of at least  $\sim 3$  kpc. In Section 3.3 we will return to the question of the physical extent of stellar mass growth, using the overlap between

<sup>&</sup>lt;sup>2</sup> There are a handful of duplicates between the UNIONS and DECaLS surveys due to overlapping declination; these are removed from the final sample.

 $<sup>^3</sup>$  We note that although we have used the combined UNIONS + DECaLS catalogs from MUMMI for this work, we see an identical signal (median  $\Delta M_{\star,fibre} = 0.04$  dex) if we use just one of these catalogs, just with fewer statistics.

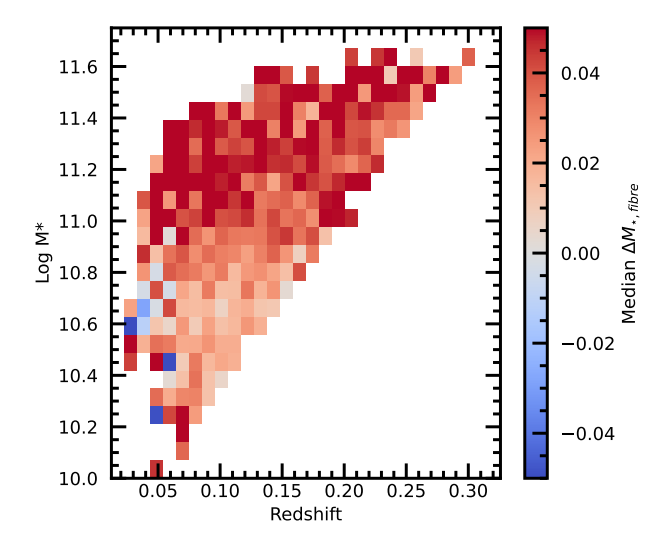


Fig. 2.— The median values  $\Delta M_{\star,fibre}$  for the post-mergers computed in bins of redshift and stellar mass. The enhancement in fibre stellar mass for post-mergers seen in Figure 1 is present across the full stellar mass and redshift range of the sample.

MaNGA and MUMMI.

## 3.2. Enhancements in bulge stellar mass

In order to move beyond the fixed angular measurement offered by  $\Delta M_{\star,fibre}$ , we now consider a more physically motivated metric. Specifically, we make use of the bulge and disk masses presented in the catalog of Mendel et al. (2014). Although galaxy mergers are typically characterized by their disturbed morphologies, our late stage post-merger sample shows only low surface brightness tidal features (see examples in Ferreira et al. 2025b). Moreover, the central stellar bulge is still well-defined in all cases that we visually inspected. Therefore, whilst measurements relating to the stellar disk may be somewhat affected by the interaction in our late-stage sample, the bulge fits (with a fixed Sersic index of  $N{=}4$ ) should be robust.

A small fraction of our post-merger sample is not included in the Mendel catalog, reducing the sample from 13,845 to 13,506. Control matching for this sample proceeds following the description in Section 2.3, i.e. matching in total stellar mass, redshift and SFR. The bulge mass offset  $(\Delta M_{\star,bulge})$  is then defined as the difference (in log space) between the bulge mass of a given post-merger and the median bulge mass of its matched control sample. In Figure 3 we show the distribution of  $\Delta M_{\star,bulge}$  for non-mergers (blue) and post-mergers (red). As expected, the non-merger distribution is centred around zero. However, the distribution of  $\Delta M_{\star,bulge}$  in the post-merger sample is skewed to positive values, with a median of 0.09 dex, corresponding to a  $\sim 20\%$  enhancement.

# 3.3. Enhancements in central stellar mass using MaNGA

Our final test of central stellar mass growth in postmergers utilizes the highest spatial resolution mass information at our disposal, namely the overlap between MUMMI and the MaNGA survey. Of the  $\sim 10{,}000$  galaxies in the final MaNGA data release, there are 177 objects in

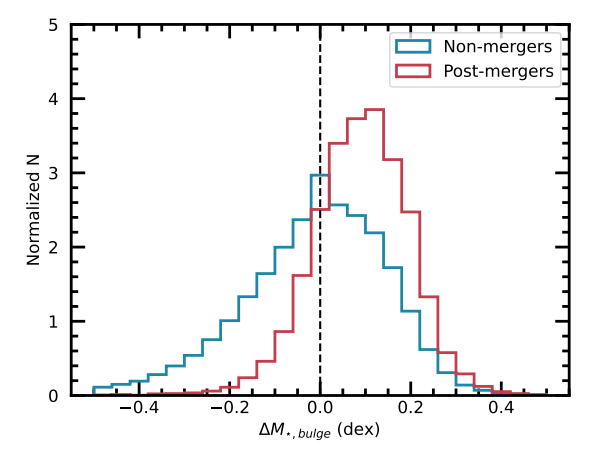


Fig. 3.— Normalized distribution of bulge stellar mass offset  $(\Delta M_{\star,bulge})$  for late-stage (0.96 <  $T_{PM}$  < 1.76 Gyr,) quenched post-mergers (red histogram) and non-mergers (blue). The vertical dashed line is at zero. The median  $\Delta M_{\star,bulge}$  for the post-mergers is 0.09 dex, corresponding to a  $\sim$  20 % enhancement.

common with our parent sample of 13,845 quenched postmergers with log  $(M_{\star}/M_{\odot}) > 10$  and  $0.96 < T_{PM} < 1.76$  Gyr. However, in order to ensure adequate resolution for our spatially resolved tests, we further restrict the sample to the 61 targets at  $z \leq 0.05$ . Given the median resolution of 2.5 arcseconds of the MaNGA survey, we therefore expect to achieve a physical resolution of at least  $\sim 2$  kpc.

We use the publically released MaNGA DR7 data products for the work presented here. Specifically, the stellar mass surface density  $(\Sigma_{\star})$ , measured in each 0.5 arcsecond spaxel, is taken from the PIPE3D catalog (Sánchez et al. 2022)<sup>4</sup>. In order to correct for inclination effects, we compute the de-projected galactocentric distance of each spaxel (in units of kpc), and also adopt inclination corrected  $\Sigma_{\star}$  values throughout the analysis that follows.

Not only is the size of our post-merger limited by the MaNGA overlap, but so too is the non-merger control pool, which contains  $\sim 5800$  galaxies. We therefore adjust our control matching methodology to take just the five best matched non-merging control galaxies for each post-merger. These best matched controls are assessed simultaneously in SFR, redshift and stellar mass using a KDTree. Due to the smaller dynamic range of redshift compared to SFR and stellar mass, the three variables are normalized before the matching process, so that they have equivalent weights. As a result, the redshift, stellar mass and SFR are typically matched to within 0.001, 0.1 dex and 0.1 dex, respectively.

For each post-merger and its five matched control galaxies, we sum  $\Sigma_{\star}$  within fixed galactocentric distances (i.e. within apertures). To avoid any *a priori* assumption of the scale on which central stellar mass growth occurs during the merger event, we compute masses in apertures with sizes from 2 up to 16 kpc (recall that,

<sup>&</sup>lt;sup>4</sup> Although the initial mass function (IMF) used in PIPE3D differs from that used in both Mendel et al. (2014) and Kauffmann et al. (2003), the differential nature of our mass analysis is agnostic to any choice of IMF.

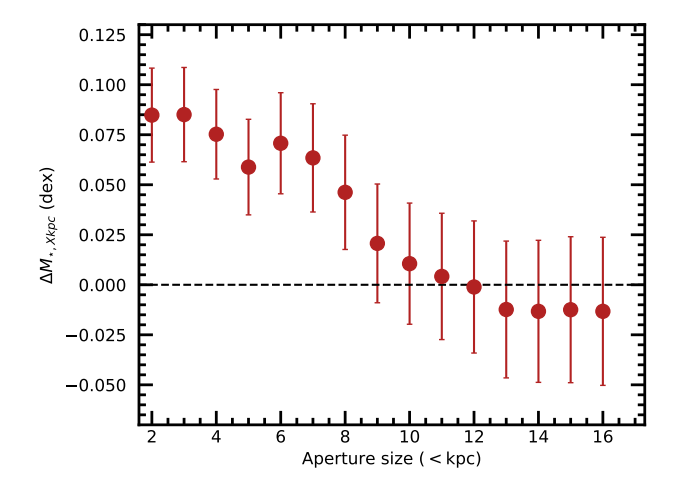


Fig. 4.— The excess mass measured using the 61  $z \le 0.05$  quenched late-stage MUMMI post-mergers with MaNGA observations. The median mass excess is computed in apertures of increasing size relative to the five best matched control galaxies. Error bars are calculated as the standard error on the median. We find that, for apertures with sizes less than  $\sim 7$  kpc, there is an approximately 15 – 20 % mass enhancement in the post-mergers.

due to our redshift cut, we expect a physical resolution of at least  $\sim 2$  kpc). The stellar mass excess,  $\Delta M_{\star,Xkpc}$ , is then computed as the difference (in log space) between the summed stellar mass within X kpc in the post-merger and the median value of the summed stellar masses within the same aperture of the matched control sample. In Figure 4 we plot the median stellar mass excess of post-mergers in bins of increasing aperture size, with uncertainties calculated as the standard error on the median. For apertures less than  $\sim 7$  kpc the typical  $\Delta M_{\star,Xkpc} \sim 0.06 - 0.08$  dex, indicating an approximately 15-20% stellar mass enhancement. This offset decreases towards larger radii; for apertures larger than 11 kpc no offset is measured.

Figure 4 hints that the stellar mass growth in late stage post-mergers is extended well beyond the central region. For reference, for stellar masses represented in our postmerger sample, the typical Petrosian r-band half light radius (as measured in NSA Atlas) is  $\sim 5$  kpc. Whilst measurements within apertures affords a maximum sample size (i.e. all 61  $z \le 0.05$  MaNGA post-mergers have  $\Delta M_{\star,Xkpc}$  measurements), interpreting the exact scale of the merger induced stellar mass growth is non-trivial, because a positive signal within a given aperture can occur even if the actual growth is on a smaller scale. We therefore repeat our calculation of  $\Delta M_{\star,Xkpc}$  but now use annuli instead of apertures. We set the width of each annulus to be 2 kpc, which approximately matches the physical resolution of the MaNGA data for the low redshift cut we have imposed. Furthermore, we require that, for the calculation of  $\Delta M_{\star,Xkpc}$  in a given annulus, 1) the post-merger must have at least five spaxels with measured  $\Sigma_{\star}$  and 2) at least three of its controls must also have measured  $\Sigma_{\star}$  in that annulus. If either of these criteria are not fulfilled, the post-merger is dropped from the sample. An increasing number of galaxies are lost as a result of insufficient spaxel coverage towards larger radii. For example, in the 9-11 and 11-13 kpc apertures only 38 and 25 of the original 61 post-mergers have MaNGA coverage, leading to larger measurement uncertainties at

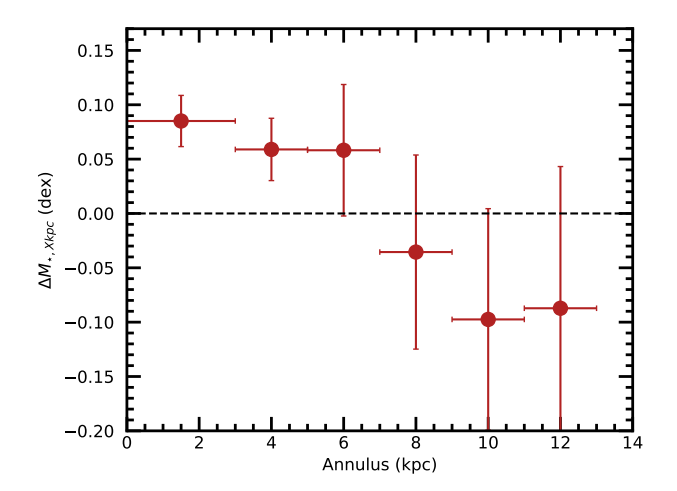


Fig. 5.— The median stellar mass excess measured in annuli. Error bars are calculated as the standard error on the median. Significant stellar mass excesses are measured in annuli up to 7 kpc from the galaxy centre.

these radii.

Figure 5 shows the  $\Delta M_{\star,Xkpc}$  for our annulus calculations. Positive stellar mass excesses with  $\Delta M_{\star,Xkpc} \sim$ 0.07 dex are measured from the centre out to a maximum annulus of 5-7 kpc. At larger radii, there is a hint of reduced stellar mass in the post-mergers, although the error bars are large and the signal is not statistically significant. Nonetheless, all three larger annuli (7-9, 9-11 and 11-13 kpc) have  $\Delta M_{\star,Xkpc} < 0$  and if we sum the signal across them all the negative mass offset does become statistically significant. We spectulate that this may be due to disruption of the stellar disk into tidal tails and shells, that remove mass at these radii. Figure 5 also explains why we start to see a decline in the stellar mass offsets for apertures larger than 7 kpc (Figure 4), i.e. because these larger apertures combine a central enhancement (at radii less than about 7 kpc) with reduced mass profiles at larger galactocentric distances. The inner enhancement is sufficiently 'diluted' once apertures larger than  $\sim 11$  kpc are measured that no mass excess is measured.

## 4. DISCUSSION AND CONCLUSIONS

Galaxy mergers have long been known to experience elevated star formation rates (Ellison et al. 2008; Barton et al. 2010; Patton et al. 2013), and recent IFU surveys have confirmed that these enhancements are centrally concentrated (Barrera-Ballesteros et al. 2015; Pan et al. 2019; Thorp et al. 2019). However, assessing the stellar mass that results from these starbursts is observationally challenging, and very few studies have reported quantitative measurements of the so-called 'burst mass fraction'. Here, we briefly review the main previous empirical attempts to measure this merger-induced mass growth, and place our own measurement in context.

Early attempts to measure the burst mass fraction relied on quantifying cusps in the central light profile that departed from the  $r^{1/4}$  law expected for the centres of merger remnants (Mihos & Hernquist 1994). Whilst analyses of merger light profiles established the presence of a 'excess' of central light (e.g. Hibbard & Yun 1999;

Rothberg & Joseph 2004), converting this to a mass fraction requires accurate modelling of the underlying disk profiles. Through careful calibration with simulations, Hopkins et al. (2008) were able to determine a stellar mass growth of 3-30~%.

The maturity of spectral fitting, derivation of star formation histories and forward modelling techniques has allowed a complementary approach to measuring merger-induced stallar mass growth. Although the details of sample selection and model fitting vary, studies employing stellar population synthesis methods have found  $\sim$  10 – 20 % mass enhancement in merger remnants (Yoon, Ko & Kim 2023; Reeves & Hudson 2024).

Finally, large galaxy surveys are now approaching both the size and image quality where it might be possible to measure the additional mass created in mergers through an enhanced gravitational lensing signal. Cheng et al. (2025) used r-band imaging from UNIONS (Gwyn et al. 2025) coupled with the original MUMMI post-merger sample of Ferreira et al. (2024) to put an upper limit on the extra mass fraction at 60 %. Larger merger samples are evidently still needed in order to produce a measurable excess lensing signal, which will likely be forthcoming, e.g. with Euclid.

The ability of MUMMI to assign a timescale to a given post-merger has now opened up a further new route to measuring the *in-situ* mass contribution from a mergerinduced starburst, and one that is arguably much simpler than previous efforts. By integrating under the curve of SFR enhancement vs. time since merger, Ferreira et al. (2025a) determined that post-mergers with  $\log (M_{\star}/M_{\odot})$ > 10 host 10-20 % more stellar mass than their mass matched controls. This method requires no modelling or choice of priors and has no intrinsic population degenaracies. It does, however, only produce a population average result and also assumes that star formation rates follow smooth (rather than highly stochastic) trajectories. If, on the other hand, merger induced star formation is bursty and highly stochastic, interspersed with extended periods of 'normal' SFRs, the 10-20 % burst mass fraction predicted by Ferreira et al. (2025a) could be an over-estimate.

In the work presented here, we have conducted a complementary analysis to the one presented in Ferreira et al. (2025a), using a sample of post-merger galaxies predicted by MUMMI to have recently completed their merger-induced burst. However, we extend the sample of post-mergers used in Ferreira et al. (2025a) by applying the MUMMI models to DECaLS r-band imaging, as well as the original UNIONS sample. As a result, our post-merger sample contains almost 14,000 quenched, late-time post-mergers for which we can conduct an measurements of stellar mass growth using SDSS imaging and spectroscopy. Moreover, 61 of these post-mergers are in

the final MaNGA data release at  $z \leq 0.05$ , allowing a more spatially resolved analysis.

By measuring enhancements in the fibre stellar mass  $(\Delta M_{\star,fibre})$ , Figure 1), bulge stellar mass  $(\Delta M_{\star,fiblee})$ , Figure 3), or within a fixed physical radius  $(\Delta M_{\star,Xkpc})$ , Figure 4) we find consistent burst mass fractions of 10 – 20 % from all three methods. This work extends that of Ferreira et al. (2025) by making a direct measurement of excess stellar mass, and allowing us to do so on a galaxy-by-galaxy basis, without any assumption on its star formation history. The excellent agreement between our work and that of Ferreira et al. (2025a) supports its implicit assumption of smooth star formation decline from the moment of coalescence to  $T_{PM} \sim 1$  Gyr.

The overlap between our MUMMI post-merger sample and the final data release of MaNGA enables us to further quantify not only the magnitude but also the physical extent of the stellar mass enhancement. Merger-induced starbursts are frequently referred to as 'central', and indeed simulations generally find enhancements within the central  $\sim$  kpc (e.g. Hopkins et al. 2008; Moreno et al. 2015, 2021). It may therefore seem surprising that we measure an excess of stellar mass in post-merger remnants even within MaNGA annuli as large as 7 kpc (Figure 5), corresponding to about  $1.4 R_e$  for the typical stellar masses in our sample. One possible explanation for this extended stellar mass excess is that some of the signal within these larger annuli could be classical ex-situ mass, i.e. stars accreted from the merging companion that settle within the disk (e.g. Angeloudi et al. 2025). On the other hand, measurements of SFR enhancements in galaxy mergers using IFU samples find that, although the starburst is centrally concentrated, enhancements are seen throughout the disk (Pan et al. 2019; Thorp et al. 2019, 2024). Our finding of  $\sim 10 \%$  enhancements in stellar mass in annuli out to 7 kpc is completely consistent with these IFU-based measurements of SFR enhancement, without the need to invoke a contribution from accreted stars. Moreover, using a sample of 31 postmergers mapped in CO(2-1) with the KILOGAS survey (Davis et al., in prep), Ledger et al. (in prep) have found molecular gas enhancements also extend out to at least 4 kpc. Taken together, the measurements of enhancements in molecular gas (Ledger et al., in prep), star formation rate (Pan et al. 2019; Thorp et al. 2019, 2024) and stellar mass (this work), paint a picture in which galaxy mergers lead to growth in both gas and stars over extents of at least the effective radius, significantly larger than is generally predicted in simulations.

In summary, the work presented here demonstrates that merger-triggered star formation can contribute an additional 10-20~% to the stellar mass of a galaxy over galactocentric radii up to 7 kpc.

## REFERENCES

Abazadjian, K. N., et al., 2009, ApJS, 182, 543 Angeloudi, E., Falcon-Barroso, J., Huertas-Company, M., Boecker, A., Sarmiento, R., Eisert, L., Pillepich, A., 2024, NatAs, 8, 1310 Angeloudi, E., Huertas-Company, M., Falcon-Barroso, J., Perreault-Levasseur, L., Adam, A., Boecker, A., 2025, A&A, in press Barrera-Ballesteros, J. K., et al., 2015, A&A, 579, 45

Barton, E. J., Geller, M. J., & Kenyon, S. J., 2000, ApJ, 530, 660

Bickley, R. W., Ellison, S. L., Patton, D. R., Bottrell, C., Gwyn, S., Hudson, M., 2022, MNRAS, 514, 3294

Boecker, A., Leaman, R., van de Ven, G., Norris, M. A., Mackereth, J. T., Crain, R. A., 2020, MNRAS, 491, 823

Boecker, A., Neumayer, N., Pillepich, A., Frankel, N., Ramesh, R., Leaman, R., Hernquist, L., 2023, MNRAS, 519, 5202

Bottrell, C., et al., 2019, MNRAS, 490, 5390

Brinchmann, J., Charlot, S., White, S. D. M., Tremonti, C., Kauffmann, G., Heckman, T., Brinkmann, J.,2004, MNRAS, 351, 1151

Cai, R., Zhu, L., Shen, S., Wang, W., Pillepich, A., Falcon-Barroso, J., 2025, A&A, 695, 177

Cannarozzo, C., et al., 2023, MNRAS, 520, 5651

Cheng, I., et al., 2025, ApJ, 992, 171

Cox, T. J., Jonsson, P., Primack, J. R., Somerville, R. S., 2006, MNRAS, 373, 1013

Cox, T. J., Jonsson, P., Somerville, R. S., Primack, J. R., Dekel, A., 2008, MNRAS, 384, 386

Ellison, S. L., Patton, D. R., Simard, L., McConnachie, A. W., 2008 AJ, 135, 1877

Ellison, S. L., Patton, D. R., Simard, L., McConnachie, A. W., Baldry, I. K., Mendel, J. T., 2010, MNRAS 407, 1514.

Ellison, S. L., Mendel, J. T., Patton, D. R., Scudder, J. M., 2013, MNRAS, 453, 3627

Ellison, S. L., Ferreira, L., Wild, V., Wilkinson, S., Rowlands, K., Patton, D. R., 2024, OJAp, 7, 121

Ellison, S. L., 2025, OJAp, 8, 12

Ferreira, L., et al., 2024a, MNRAS, 533, 2547

Ferreira, L., et al., 2025, MNRAS, 538, L31

Ferreira, L., et al., 2025b, MNRAS, submitted

Gwyn, S. J., et al., 2025, AJ, 170, 324

Hani, M. H., Gosain, H., Ellison, S. L., Patton, D. R., Torrey, P., 2020, MNRAS, 493, 3716

Hibbard, J. E., & Yun, M. S., 1999, AJ, 118, 162

Hopkins, P. F., Hernquist, L., Cox, T. J., Dutta, S. N., Rothberg, B., 2008, ApJ, 679, 156

Karademir, G. S., et al., 2019, MNRAS, 487, 318

Kauffmann, G., et al., 2003, MNRAS, 341, 33

Koppula, S., et al. 2021, arXiv e-prints, arXiv:2102.05182 Lambas, D. G., Tissera, P. B., Alonso, M. S., Coldwell, G.,

2003, MNRAS, 346, 1189 Lambas, D. G., Alonso, S., Mesa, V., O'Mill, A. L., 2012, A&A, 539, 45

This paper was built using the Open Journal of Astrophysics LaTeX template. The OJA is a journal which

Mendel, J. T., Palmer, M. J. D., Simard, L., Ellison, S. L., Patton, D. R., 2014, ApJS, 210, 3

Mihos, C., & Hernquist, L., 1994, ApJ, 437, L47

Moreno, J., Torrey, P., Ellison, S. L., Patton, D. R., Bluck, A. F. L., Bansal, G., Hernquist, L., 2015, MNRAS, 448, 1107 Moreno, J., et al 2021, MNRAS, 503, 3113

Nelson, D., et al., 2019, ComAC, 6, 2

Nikolic, B., Cullen, H., Alexander, P., 2004, MNRAS, 355, 874 Pan, H.-A., et al., 2019, ApJ, 881, 119

Patton, D. R., Ellison, S. L., Simard, L., McConnachie, A. W., Mendel, J. T., 2011, MNRAS, 412, 591

Patton, D. R., Torrey, P., Ellison, S. L., Mendel, J. T., Scudder, J. M., 2013, MNRAS, 433, L59

Patton, D. R., et al., 2020, MNRAS, 494, 4969

Pearson, W. J., Rodriguez-Gomez, V., Kruk, S., Margalef-Bentabol, B., 2024, A&A, 687, 45

Pearson, W. J., Wang, L., Rodriguez-Gomez, V.,

Margalef-Bentabol, B., Suelves, L. E., 2025, A&A, in press Perez, M. J., Tissera, P. B., Lambas, D. G., Scannapieco, C., 2006, A&A, 449, 23

Reeves, A., & Hudson, M., 2024, MNRAS, 527, 2037

Rodriguez-Gomez, V., et al., 2016, MNRAS, 458, 2371 Rothberg, B., & Joseph, R. D., 2004, AJ, 128, 2098

Rothberg, B., & Joseph, R. D., 2004, AJ, 128, 2098

Sanchez, S. F., et al., 2022, ApJS, 262, 36 Schechter, A., et al., 2025, ApJ, 989, 149

Scott, C., & Kaviraj, S., 2014, MNRAS, 437, 2137

Steffen, J. L., Fu, H., Comerford, J. M., Dai, Y. S., Feng, S., Gross, A. C., Xue, R., 2021, ApJ, 909, 120

Torrey, P., Cox, T. J., Kewley, L. J., Hernquist, L., 2012, ApJ, 746, 108

Thorp, M. D., Ellison, S. L., Simard, L., Sanchez, S. F., Antonio, B., 2019, MNRAS, 482, L55

Thorp, M. D., Ellison, S. L., Galicia, A., 2024, A&A, 690, L4 Valenzuela, L. m., & Remus, R.-S., 2024, A&A, 686, 182

Vasquez-Bustos, P., Argudo-Fernandez, M., Boquien, M., Castillo-Baeza, N., Castillo-Rencoret, A., Ariza-Quintana, D., 2025, A&A, 696, 206

Wilkinson, S., Ellison, S. L., Bottrell, C., Bickley, R. W., Byrne-Mamahit, S., Ferreira, L., Patton, D. R., 2024, MNRAS, 528, 5558

Yoon, Y., Ko, J., Kim, J.-W., 2023, ApJ, 946, 41

provides fast and easy peer review for new papers in the astro-ph section of the arXiv, making the reviewing process simpler for authors and referees alike. Learn more at http://astro.theoj.org.